MODELLING OF BEARING LUBRICATION FOR ELECTRIC VEHICLE MOTOR BEARING

Siti Hartini Hamdan[a]*, Chiew Tin Lee[b], Jian Hao Ng[c]

[a]Malaysian Institute of Chemical and Bioengineering Technology (MICET), Universiti Kuala Lumpur, 78000 Alor Gajah, Melaka, Malaysia
[b]Faculty of Engineering, Universiti Malaysia Sarawak (UNIMAS), Kota Samarahan 94300, Sarawak, Malaysia
[c]Faculty of Mechanical Engineering, Universiti Teknologi Malaysia, 81310 UTM Johor Bahru, Johor, Malaysia

Article history
Received
5th January 2025
Received in revised form
10th March 2025
Accepted
10th June 2025
Published
26th June 2025

*Corresponding author
sitihartini@unikl.edu.my

ABSTRACT

Bearing failure in electric motors is increasingly attributed to complex electro-thermal interactions that accelerate surface damage and lubricant degradation. Electrical current discharge disrupts the lubricant's rheological properties, diminishing film thickness and undermining protection in the elastohydrodynamic lubrication regime. This study presents a numerical model that integrates EHL theory with heat generation from shear and electrical sources while capturing the influence of key operating parameters such as shaft speed, bearing resistivity, and temperature. The findings reveal that current discharge markedly reduces minimum film thickness and distorts pressure distribution due to localised temperature rise and viscosity breakdown. The model demonstrates strong predictive capability by capturing the coupled effects of entrainment, rheological degradation, and electro-thermal loading. These results underscore the sensitivity of EHL film formation to electrical stress and highlight potential failure thresholds under realistic operating conditions. The insights gained can inform the development of advanced bearing systems with enhanced thermal management, electrical insulation, and lubricant formulation strategies, ultimately improving the durability and reliability of electric motor drivetrains.

KEYWORDS

Point Contact, Elastohydrodynamic (EHL), Current Discharge, Electric Vehicle.

INTRODUCTION

In recent years, electric vehicles (EVs) have gained significant attention as a technology to meet climate targets. The development of EVs has been accelerated with the introduction of subsidies for sustainable automotive technologies worldwide. However, several challenges and concerns still need to be addressed. One of these challenges lies in the field of lubricants, which play a critical role in ensuring the performance and reliability of EVs, particularly in bearing lubrication.

Bearing failures in electric motors are often linked to multiple interrelated phenomena such as lubricant thermal degradation, oxidation, contamination, and especially electrical discharge effects. Electrical discharge causes localized high temperatures that degrade lubricant chemistry, reduce viscosity, and lead to surface pitting or fluting [1,5]. Studies have shown that over 40% of bearing failures in EVs are due to electrical current-related effects [1], making this a major reliability concern. While thermal and tribological degradation mechanisms have been extensively studied, the coupling of electrical current with EHL behaviour remains insufficiently explored. This motivates the need for a simulation framework that integrates current discharge into EHL modelling to better predict film breakdown and performance loss in EV applications.

Approximately 40% of electric motor failures in EVs are attributed to bearing failure, often caused by complex voltage and current conditions [1]. This leads to damage and failure of both the bearing and the lubricant. To tackle this issue, research efforts are necessary to develop lubricants specifically designed to meet the unique challenges of EVs.

EV lubricants encounter several challenges, such as the demand for high-speed and high-temperature capabilities, strong electrical

conductivity, corrosion resistance, and comprehension of tribological performance across various operating conditions [2]. In lubricated interfaces, electrical contacts often undergo triboelectric charging due to frictional interactions between surfaces, resulting in the accumulation of electrostatic charges and thermal effects [3,4]. This issue can impair friction and wear properties, accelerate oxidation, and cause damage from electrostatic discharge. A recent study by Mohamed Ariffin et al. [5] revealed that greases with low interfacial resistance can maintain their lubrication effectiveness under triboelectric conditions.

This study aims to determine the variation in minimum film thickness in a bearing model of an electric vehicle under elastohydrodynamic lubrication conditions influenced by current discharge. By incorporating the principles of elastohydrodynamic lubrication and heat generation resulting from shearing and current, a numerical model will be employed to investigate the behaviour of the lubrication system and provide accurate predictions for practical applications.

This study builds upon established theoretical models widely used in elastohydrodynamic lubrication analysis. The Reynolds equation serves as the core for film thickness and pressure distribution, with viscosity and density variations captured using Roelands' and Dowson–Higginson's models, respectively [6,7]. Heat generation from shearing follows the classical wedge and shear energy balance approach [6], while electrical discharge heating is modelled using resistive energy conversion equations adapted from prior studies on bearing arcing [8,9]. These formulations form the basis of the coupled electro-thermal EHL simulation developed herein.

Unlike conventional internal combustion engine vehicles, EVs are subject to electrical current discharge within motor bearings, making electro-thermal effects a critical design and lubrication challenge. This study specifically addresses these unique EV conditions. Although prior EHL studies have extensively modelled film formation under mechanical and thermal loads, they often neglect the effects of electrical discharge—an increasingly critical failure mode in EV bearings. Therefore, this study aims to fill that gap by developing a simulation framework that couples electrical, thermal, and mechanical effects to better understand lubrication behavior in electrified drivetrains.

THEORETICAL FORMULATION

2-D Reynolds Equation

The contact pressure distribution and the lubricant film profile from point-contact under elastohydrodynamic lubrication can be described using the Reynolds equation as in Equation (1). In this study, the non-dimensionalisation follows the one given in reference [6].

$$\frac{\partial}{\partial X}\left(\frac{\bar{\rho}H^3}{\bar{n}}\right)\frac{\partial P}{\partial X}+k^2\frac{\partial}{\partial Y}\left(\frac{\bar{\rho}H^3}{\bar{n}}\right)\frac{\partial P}{\partial Y} = \Psi\left\{\left(\frac{\partial(\bar{\rho}\mathrm{HU})}{\partial \mathrm{X}}\right)+k\left(\frac{\partial(\bar{\rho}\mathrm{HV})}{\partial \mathrm{Y}}\right)\right\} \quad (1)$$

$x=bX;\ y=aY;\ \rho=\rho_o\bar{\rho}\ ;\ \eta=\eta_o\bar{\eta}\ ;\ h=\frac{Hb^2}{R}\ ;$
$p=P_hP;\ u=u_{av}U;\ v=v_{av}V$

where; $\Psi=12\frac{u_{av}\eta_oR_x^2}{P_hb^3}$; $k=\frac{b}{a}$

Equation (2) is the Reynolds equation for determining the dimensionless pressure *"P"*. However, before proceeding, the dimensionless film thickness *H,* the dimensionless density $\bar{\rho}$, and the dimensionless viscosity $\bar{n}$ will need to be expressed.

Lubricant Rheological Properties

The density and viscosity of lubricants, especially viscosity, changes with pressure and temperature. The density depends also on these factors, aligning with the established relationship described by Dowson and Higginson [7], as mentioned in Equation (3). In contrast, the viscosity of the lubricant shows considerable sensitivity to variations in both pressure and temperature. For medium to high pressures encountered in elastohydrodynamic contacts, the relationship put forth by Roelands in Equation (4) is suitable.

$$\rho_{i,j}=\rho_o\left(1+\frac{0.6x10^{-9}p}{1+1.7x10^{-9}p}\right)-D_t\,(\theta-\theta_i) \quad (2)$$

$$\eta_{i,j} = \eta_o exp\left\{[9.67+ln\eta_o]\left[-1+(1+5.1\,x\,10^{-9}\,p)^{z'}x\,(\frac{\theta-138}{\theta_i-138})^{-S_o}\right]\right\} \quad (3)$$

where the contact temperature $\theta\ (K)=\theta_i+\Delta\theta+273$ while S_0 can be determined using:

$$S_o = \beta\left(\frac{\theta_i - 138}{ln\, n_o + 9.67}\right)$$
$$z' = \frac{\alpha}{5.1\ x\ 10^{-9}\ (\ln n_o + 9.67)}$$

Elastic Film Shape

In a ball bearing, the elastohydrodynamic film resembles a parabolic curve. This curve illustrates the interaction between a flat, semi-infinite elastic half-space and the localised Hertzian contact deformation. With the initial gap of h_o, the elastic film shape for a ball bearing is [6]:

$$h(x,y) = h_o + \frac{x^2}{2R} + \frac{y^2}{2R} + d_e \quad (4)$$

The term d_e is the local deformation. It is solved analytically following the cumulative effect of pressure element p_{ij} contributing to the deflection at point k, l. The solution yields an influence coefficient that evaluates contact deflection by the superposition principle.

Heating Effect

Shearing and Wedge Effect

The lubricant shear within the contact region, along with the pressure gradient resulting from the wedge effect, generates heat. In elastohydrodynamic films, conduction through the contact surface dominates convection heat transfer [4]. Consequently, the convection heat transfer can be neglected in the current analysis. Additionally, for this analysis, the side leakage is considered insignificant. Taking these factors into account, the energy equation for heat transfer can be simplified to Equation (5) as follows:

$$u\theta\alpha'\left(\frac{\partial p}{\partial x}\right) + \emptyset\ \left(\frac{\partial u}{\partial z}\right)^2 = -k'\frac{\partial^2\theta}{\partial z^2} \quad (5)$$

The temperature variation is assumed to be linear, expressed as $\Delta\theta/h$. The heat removed by conduction at the top surface within the contact can be represented as $bk\Delta\theta/h$. The superposition approach is applied to the left-hand side of Equation (5).

Additionally, a linear velocity variation across the lubricating film is assumed to analyse viscous heating. By employing these assumptions and considerations, an analytical solution is obtained in Equation (6), calculating the temperature rise. This solution provides insights into the system's thermal behaviour and enables the assessment of temperature-related factors in elastohydrodynamic lubrication [6].

$$\Delta\theta = \left[\frac{u_{av}\theta_i\alpha' hp + (2bn_o{u_{av}}^2/h)}{(bk'/h) - u_{av}\alpha' hp}\right] \quad (6)$$

Current Discharge

When the electrical current passes through the inner race ball track and a ball in a bearing, it generates heat instantaneously. With the current, I flowing through the contact with electrical resistance, R for a duration, t_{ob}, the amount of electrical energy produced can be calculated using Equation (7):

$$q_{ir} = I^2 R t_{ob} \quad (7)$$

This electrical energy influences the contact are, which is the circle circumference formed by the width of the corrugation (πW_{ob}), contact arc length on the ball track of outer race (L_{ob}) and corrugations depth (H_c). As a first approximation, isolating other modes of heat transfer, the instantaneous temperature rise during each contact of a ball with the inner race ball track is determined using Equation (8) [8]:

$$\pi W_{ob} L_{ob} H T_{ob} \rho_b c_b = I^2 R t_{ob} \quad (8)$$

Equation (8) is further derived to obtain the temperature rise at each contact of a ball with the outer race ball track as in Equation (9):

$$T_{ob} = \frac{5.8 I^2 R_b K D(D+2d)}{f_s H_c \rho_b c_b \alpha'' d(D+d)(D^2 - d^2 cos^2\alpha'')} \quad (9)$$

A single ball contact position, which passes the circumferential length, $\pi(D+d)/2$, is referred to as the instant maximum loaded zone of the outer race ball track. This takes $(D+d)/(2f_b d)$ seconds to complete. Subsequently, for a ball completes a single rotation on the outer race ball track, a time of $1/f_b$ seconds is required. So, in $1/2f_s$ seconds, the time taken for the inner race to pass through the loaded zone for a single position on a ball contacting the outer race ball track $f_b/2f_s$ seconds.

Therefore, the instantaneous temperature rises of the outer race ball track attributed to the single position ball contacts in each shaft rotation would be $f_b/2f_s$ times the T_{ob}, giving Equation (10), which is then added to Equation (7) in attaining the instantaneous temperature rise for the contact.

$$T_{obn} = \frac{1.45 I^2 R_b K(D+2d)}{f_s H_c pc\alpha d^2(D+d)} \quad (10)$$

Load Balance

The total load is obtained by integrating the pressure across the contact width. The load needs to equal the external force exerted on the contacting surface.

$$\int_{-\infty}^{+\infty} p\, dxdy = w \tag{11}$$

Mathematical Solution

A simultaneous solution for Equations (1)-(4), (6), (10) and (11) is needed. The proposed solution utilises the Newton–Raphson method, incorporating Gauss–Seidel iterative method [6]. The contact pressure at iteration is:

$$P_{i,j}^{n} = P_{i,j}^{n-1} + \Omega \Delta P_{k,l}^{n} \tag{12}$$

Where Ω is the relaxation factor.

Two convergence criteria are required in each small time step: one for pressures *pi,j* and the other for the contact load. For pressure convergence in Equation (13), the error tolerance ε_p ≈1x10^{-5}.

$$\frac{\sum_{i=1}^{nx}\sum_{j=1}^{ny}\left|p_{i,j}^{k} - p_{i,j}^{k-1}\right|}{\sum_{i=1}^{nx}\sum_{j=1}^{ny} p_{i,j}^{k}} \ll \varepsilon_p \tag{13}$$

The following criterion is used for load convergence, with error tolerance ε_w ≈ 1x10^{-2}.

$$\frac{|w - F|}{F} \text{"} \varepsilon_w \tag{14}$$

When the criterion in Equation (14) is not achieved, the film profile is updated using the damping factor, $\vartheta \approx 1\text{x}10^{-7}$.

$$H_o^k = H_o^{k-10} + \vartheta\left(\frac{w - F}{F}\right) \tag{16}$$

Results and Discussion

Validation of Numerical Model

The numerical model is validated using the analytical model proposed by Hamrock and Dowson under isothermal conditions [7]. Figure 1 compares the numerical and analytical models, considering an entrainment speed range of 0.832 to 4.16 m/s, corresponding to shaft rotation speeds of 10,000 rpm to 50,000 rpm.

Overall, there is an acceptable agreement between the numerical and the analytical solutions for the minimum lubricant film thickness. However, the accuracy of the analytical model diminishes when the entrainment speed falls below 2.5 m/s, as the lubrication regime is likely to shift towards mixed lubrication. The analytical model is primarily intended for elastohydrodynamic lubrication and may not accurately predict behaviour along the mixed lubrication regime.

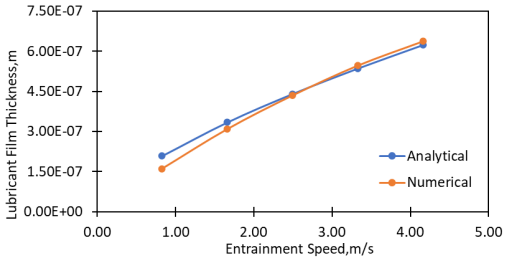

Figure 1: Lubricant film thickness versus entrainment speed

The numerical model shows good agreement with the Hamrock–Dowson analytical solution, with a maximum relative error in minimum film thickness of less than 8% across the examined entrainment speeds. According to common EHL design guidelines, a λ ratio greater than 3 is generally required to avoid asperity contact, ensuring full film lubrication.

Effect of Current on Film Thickness

The increase in lubricant average temperature, as shown in Figure 3, significantly reduces the lubricant film thickness, which is consistent with the reported findings [8]. The percentage of reduction in film thickness ranges from 57.6% to 84.8% as given in Figure 2. Moreover, this reduction becomes more pronounced with increasing current. The decrease in minimum film thickness, as summarised in Figure 4, can be attributed to the decrease in lubricant viscosity caused by the elevated temperature [8].

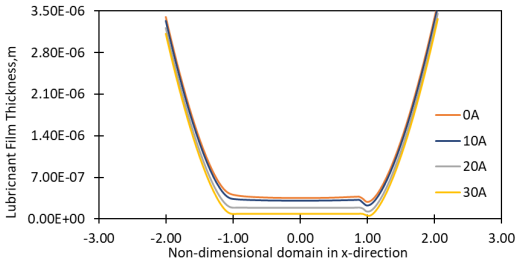

Figure 2: Lubricant film thickness versus non-dimensional domain in x-direction

The rise in temperature becomes more significant with higher entrainment speeds [8]. Additionally, heat is generated when current passes through the inner race ball track and a ball. The voltage exceeding a certain threshold results in a rapid increase in current flow [9]. This electric motor breakdown can occur due to shaft voltage [1]. The combined effects of current and shearing lead to increased heat generation, resulting in a more pronounced temperature rise and subsequent reduction in film thickness.

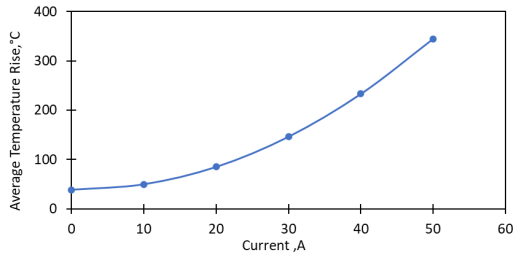

Figure 3: Lubricant average temperature rise versus electrical current

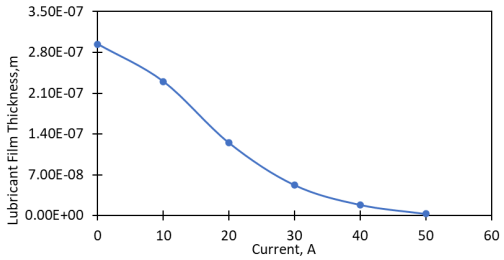

Figure 4: Lubricant minimum film thickness versus electrical current

Furthermore, the results in Figure 5 indicate that in the vicinity of the exit constriction, the pressure spike is absent due to contact starvation as the temperature rises, which is aligned with the reported data [8]. With the increase in applied current, there is a tendency for the pressure spike to diminish and move towards the exit from the contact region. Notably, when the applied current reaches 30 A, the second pressure spike almost disappears. However, the pressure distribution remains relatively similar.

Notably, when the applied current reaches 30 A, the second pressure spike almost disappears. This occurs due to significant localised heating that reduces lubricant viscosity near the exit region, resulting in film starvation and an inability to sustain the pressure gradient typically observed in fully developed EHL conditions.

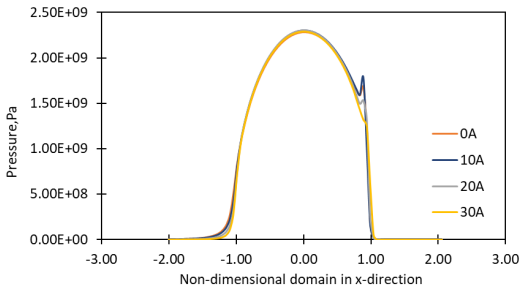

Figure 5: Contact pressure versus non-dimensional domain in x-direction

Effect of Shaft Rotational Speed with Electrical Current

Without electrical current, the entrainment effect dominates over the thermal effect induced by shearing and current within a certain range of speeds, increasing minimum film thickness (see Figure 7). However, as the shaft rotational speed increases, the thermal effect overwhelms the entrainment effects (see Figure 6), resulting in a decrease in film thickness, aligned with reported data [6].

While the trend of film thickness change remains consistent in both the presence and absence of electrical current, there are significant differences in temperature behaviour. Specifically, when electrical current is present, the average temperature rise is more prominent at lower entrainment speeds. However, an interesting phenomenon occurs as the speed increases—the temperature starts to decrease. This unexpected decrease in temperature persists until a critical speed is reached. At this critical speed, the average temperature begins to rise once again.

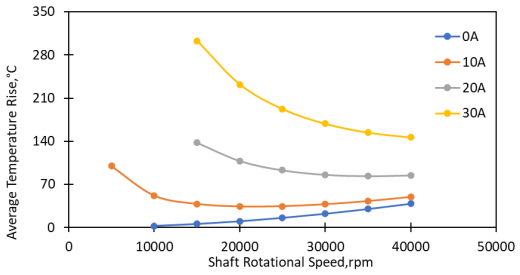

Figure 6: Lubricant average temperature rise versus shaft rotational speed

However, an interesting phenomenon occurs as the speed increases, the temperature starts to decrease. This is due to enhanced lubricant entrainment at higher speeds, which increases the convective transport of heat away from the contact region, thereby offsetting the heat generated by shearing and current discharge.

Furthermore, under different current conditions, the trend of film formation remains relatively consistent. However, higher currents require higher shaft rotational speeds to achieve film formation. Additionally, as the current increases, the rotational speed required to attain the thickest film thickness increases, as depicted in Figure 7. These findings emphasise the intricate relationship between shaft rotational speed, current influence, and film formation in elastohydrodynamic lubrication.

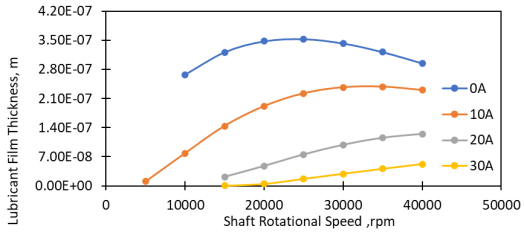

Figure 7: Lubricant minimum film thickness versus shaft rotational speed

The present model assumes steady-state electrical discharge conditions for simplicity and numerical tractability. However, actual electric motor environments often involve transient phenomena such as current spikes and intermittent arcing. These can cause localized thermal stresses, rapid lubricant degradation [10], and surface damage mechanisms not captured in this study. Future extensions should incorporate time-dependent discharge profiles, transient heat conduction, and cumulative degradation modelling to more accurately reflect real-world bearing conditions.

Effect of Lubricant Base Temperature

As the boundary temperature rises, there is a significant reduction in the lubricant minimum film thickness as depicted in Figure 8. This finding aligns with the expected behaviour of lubricants, as higher temperatures decrease viscosity. Consequently, the decrease in viscosity affects the lubricant's ability to sustain an adequate film thickness, resulting in a thinner film. It is worth noting that the trend in film thickness under the influence of current remains consistent across different boundary temperatures, indicating a uniform impact of current on the lubricant film thickness, regardless of the boundary temperature.

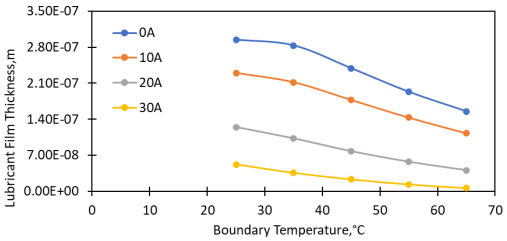

Figure 8: Lubricant film thickness versus boundary temperature

Effect of Varying Bearing Resistance

Prashad's work [9] suggests a direct proportionality between lubricant resistivity and equivalent bearing resistance. Higher resistivity lubricants result in higher bearing resistance, indicating that lubricant resistivity plays a significant role in determining the overall resistance experienced by the bearing system. Figure 9 illustrates that the increased resistance leads to a higher instantaneous temperature rise due to current, caused by resistive heating through the lubricant. As a result of this heating, the lubricant minimum film thickness decreases, as shown in Figure 10.

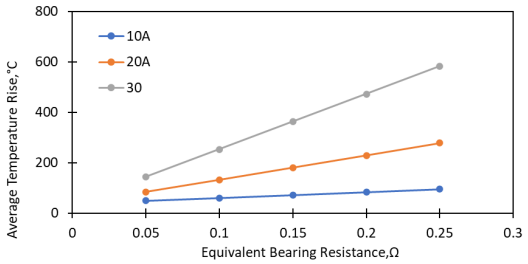

Figure 9: Lubricant average temperature rise versus equivalent bearing resistance

The trend of lubricant resistivity remains consistent across different current values, with higher resistivity lubricants consistently exhibiting higher equivalent bearing resistance. This highlights the dominant role of lubricant resistivity in determining the overall resistance of the bearing system. Moreover, Prashad's research [9] emphasises the impact of lubricant resistivity on current passage within the bearing, particularly the occurrence of arcing and potential failure. High-resistivity lubricants can lead to localised electrical breakdowns, resulting in arcing and potential damage to the bearing components.

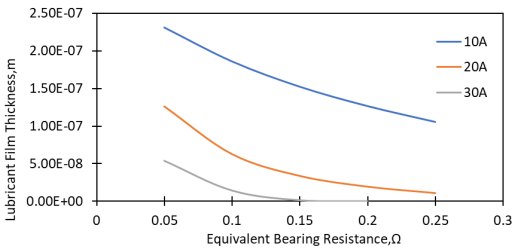

Figure 10: Lubricant minimum film thickness versus equivalent bearing resistance

Conclusion

This study investigates the behaviour of lubricated ball bearings under elastohydrodynamic lubrication (EHL) conditions when subjected to electrical current, incorporating variables such as shaft rotational speed, bearing equivalent resistivity, and boundary temperature. Results show that electrical current significantly affects lubricant film thickness and pressure distribution, with film thickness decreasing markedly as current intensity increases.

Minimum film thickness under electrical influence was determined by accounting for temperature rise, viscosity reduction, and entrainment effects. The analysis further highlights the roles of shaft speed, lubricant temperature, and equivalent bearing resistance in shaping lubrication performance.

These findings provide critical insight into how electrical current alters EHL behaviour, particularly its effect on minimum film thickness and contact pressure—key factors in preventing wear and fatigue. By identifying the conditions that lead to film breakdown, this study supports the development of optimized lubrication strategies, appropriate insulation measures, and operational controls, thereby enhancing the durability and efficiency of ball bearings in electric motor systems. While the current model captures the coupled electro-thermal effects under steady conditions, future studies should consider transient current events and their cumulative impact on long-term bearing degradation.

Acknowledgements

The authors gratefully acknowledge the valuable technical guidance of Assoc. Prof. Dr. William Woei Fong Chong from Universiti Teknologi Malaysia (UTM) in developing and deriving the numerical algorithm used in this study.

Conflict of Interest

The author declares that there is no conflict of interest regarding the publication of this paper.

References

[1] Zhang, He, F., Xie, G., & Luo, J. (2020). Electrical bearing failures in electric vehicles. *Friction, 8*(1), 4–28. https://doi.org/10.1007/s40544-019-0316-3

[2] Chen, Y., Jha, S., Raut, A., Zhang, W., & Liang, H. (2020). Performance characteristics of lubricants in electric and hybrid vehicles: A current and future needs review. *Frontiers in Mechanical Engineering, 6*, 571464. https://doi.org/10.3389/fmech.2020.571464

[3] Lee, W. B., & Orr, D. E. (2022). *The Triboelectric Effect Series*. AlphaLab, Inc. Retrieved June 30, 2024, from https://www.alphalabinc.com/wp-content/uploads/2024/02/The-Triboelectric-Effect-Series-AlphaLab-Inc.pdf

[4] Wang, J., Zhou, L., Zhang, C., & Wang, Z. L. (2019). Small-scale energy harvesting from environment by triboelectric nanogenerators. In R. Manyala (Ed.), *Small-Scale Energy Harvesting* (Chapter 4, pp. 63–94). IntechOpen. https://doi.org/10.5772/intechopen.82023

[5] Mohamed Ariffin, N. A. A., Lee, C. T., Thirugnanasambandam, A., Wong, K. J., & Chong, W. W. F. (2024). Triboelectric performance of ionic liquid, synthetic, and vegetable oil-based polytetrafluoroethylene (PTFE) greases. *Lubricants, 12*(8), 272. https://doi.org/10.3390/lubricants12080272

[6] Chong, W. W. F., Teodorescu, M., & Rahnejat, H. (2014). Mixed thermo-elastohydrodynamic cam–tappet power loss in low-speed emission cycles. *International Journal of Engine Research, 15*(2), 153–164. https://doi.org/10.1177/1468087413492841

[7] Hamrock, B. J., & Dowson, D. (1977). Isothermal elastohydrodynamic lubrication of point contacts: Part III—Fully flooded results. *Journal of Lubrication Technology, 99*(2), 264–275. https://doi.org/10.1115/1.3453115

[8] Karthikeyan, B. K., Teodorescu, M., Rahnejat, H., & Rothberg, S. J. (2010). Thermoelastohydrodynamics of grease-lubricated concentrated point contacts. *Proceedings of the Institution of Mechanical Engineers, Part C: Journal of Mechanical Engineering Science, 224*(3), 683–695. https://doi.org/10.1243/09544062JMES1654

[9] Prashad, H. (2005). *Tribology in electrical environments*. Elsevier.

[10] Ariffin, N. A. A. M., Pui, Y. H., Bao, L. M., Hamdan, S. H., & Chong, W. W. F. (2023). Tribological performance of perfluoropolyether (PFPE)-based grease for potential application in electric motor bearings. *Journal of Transport System Engineering, 6*(2), 60–65.

APPENDIX 1

Notation

a	Contact radius at x-direction (m)
b	Contact radius at y-direction (m)
c_b	Specific heat of bearing material ($Jkg^{-1}°C^{-1}$)
d	Diameter of ball (m)
D	Pitch diameter (m)
d_e	Elastic deformation (m)
D_t	Density-temperature dependency (K^{-1})
f_s	Shaft rotational frequency (Hz)
H	Dimensionless film thickness
H_c	Depth of slip bands and craters on track surfaces of races (m)
h	Film thickness (m)
h_o	Initial assumption for film thickness (m)
k'	Thermal conductivity of the lubricant (W/(m/K))
K	Number of rolling elements in loaded zone
$\bar{n}$	Dimensionless lubricant viscosity
n	Lubricant Viscosity (Pa s)
n_o	Lubricant viscosity at ambient temperature (Pa s)
P	Dimensionless pressure
P_h	Maximum hertzian pressure (Pa)
p	Contact pressure (Pa)
R	Radius of curvature
R_b	Equivalent bearing resistance (Ω)
u_a, u_b	Sliding velocity (ms^{-1})
u_{av}	Mean sliding velocity (m/s)
U	Dimensionless sliding velocity
v_a, v_b	Transverse velocity (ms^{-1})
v_{av}	Mean transverse velocity (m/s)
V	Dimensionless transverse velocity
w	Load (N)
x	Sliding direction coordinate (m)
X	Non-dimensional domain in x-direction (sliding direction)
y	Transverse direction coordinate (m)
Y	Non-dimensional domain in x-direction (transverse direction)
$\bar{\rho}$	Dimensionless density (kg/m^3)
ρ_o	Density at ambient pressure (kg/m^3)
ρ_b	Density of bearing material (kg/m^3)
θ	Temperature (K)
θ_i	Initial oil Temperature (K)
α	Pressure-viscosity coefficient (Pa^{-1})
α'	Coefficient of lubricant thermal expansion ($°C^{-1}$)
α''	Contact angle

APPENDIX 2

Simulation Input Parameter [8, 9]

Input Parameter	Unit	Value
Race radius of curvature, R_2	m	$11.28x10^{-3}$
Radius of rolling ball, R_1	m	$2.39x10^{-3}$
Elastic modulus of outer race ring	Pa	$200x10^9$
Poison Ratio of outer race ring	-	0.28
Elastic modulus of rolling ball	Pa	$200x10^9$
Poison Ratio of rolling ball	-	0.28
Density of Ball, ρ_b	Kg/m^3	$7.7x10^3$
Specific heat of bearing material, c_b	$Jkg^{-1}°C^{-1}$	$4.6x10^2$
Pitch diameter of bearing, D	m	$8.9x10^{-3}$
Depth of slip bands and craters on track surfaces of races, H_c	m	$3x10^{-6}$
Pressure-viscosity coefficient, α	Pa^{-1}	$2.08x10^{-8}$
Contact angle, α''	°	15
Coefficient of lubricant thermal expansion, α'	$°C^{-1}$	$6.4x10^{-4}$
Thermal conductivity of the lubricant,k'	W/(m/K)	$1.45x10^{-1}$
Density-temperature dependency, D_t	K^{-1}	1.15
Number of rolling elements in loaded zone	-	3
Load applied on the ball	N	27.67